scientific reports

Check for updates

OPEN

Detecting severe coronary artery stenosis in T2DM patients with NAFLD using cardiac fat radiomics-based machine learning

Mengjie Liang[1], Liting Fang[2], Xie Chen[1] & Wendi Huang[1]✉

To analyze radiomics features of cardiac adipose tissue in individuals with type 2 diabetes (T2DM) and non-alcoholic fatty liver disease (NAFLD), integrating relevant clinical indicators, and employing machine learning techniques to construct a precise model for detecting severe coronary artery stenosis. A retrospective analysis of 710 T2DM patients with NAFLD was conducted at First People's Hospital of Wenling. The study population was randomly divided into a training set (n = 497) and a validation set (n = 213). Radiomics features from cardiac fat CT images, including epicardial adipose tissue (EAT) and paracardial adipose tissue (PAT), were extracted for all patients. The semi-automated segmentation and extraction of shape, first-order statistics, texture, and wavelet were performed using specialized software. Simultaneously, clinical characteristics were collected. Following feature selection, four machine learning algorithms were utilized to develop radiomics, clinical, and combined radiomics-clinical models. The detection performance of these models was subsequently evaluated in both the training and validation cohorts. Additionally, Shapley Additive exPlanations (SHAP) values were calculated to quantify the importance of features. A total of 10 radiomics features for EAT and PAT were extracted from CT images after feature selection. The clinical model obtained an area under the curve (AUC) of 0.747 with the support vector machine (SVM), while the radiomics model reached an AUC of 0.838 with the extreme gradient boosting (XGBoost) algorithm. In comparison, the radiomics-clinical model using XGBoost demonstrated superior detection capability, achieving an AUC of 0.883 in the training set and maintaining high performance in the validation set, with the highest F1 score, accuracy, and precision. SHAP analysis revealed the importance of radiomics features from EAT and PAT, as well as clinical factors such as diabetes duration, global longitudinal strain (GLS), and low-density lipoprotein cholesterol (LDL-C), in detecting severe coronary artery stenosis. This study confirms that the integrated application of cardiac fat radiomics features and clinical data using machine learning models, particularly the XGBoost algorithm, facilitates the detection of severe coronary artery stenosis in T2DM patients with NAFLD. SHAP analysis further elucidates the contribution of key variables in the model, providing crucial foundations for personalized treatment decision-making.

Keywords Type 2 diabetes, Nonalcoholic fatty liver disease, Cardiac fat, Radiomics, Machine learning

Type 2 diabetes mellitus (T2DM) and non-alcoholic fatty liver disease (NAFLD) are prevalent metabolic disorders that demonstrate a global upward trend in incidence. The simultaneous manifestation of these conditions exacerbates lipid dysregulation, chronic inflammation, oxidative stress, and endothelial cell dysfunction, significantly increasing the incidence of severe coronary artery stenosis[1–3]. Such severe stenosis is associated with a heightened risk of myocardial ischemia and can lead to significant complications, including myocardial infarction, thus posing a serious threat to patient health[4,5]. Early and accurate detection of severe coronary artery stenosis holds substantial clinical significance for therapeutic intervention and prognosis.

In the context of metabolic disorders, excessive fat accumulation around the heart, blood vessels, kidneys, and neck can trigger various metabolic changes, elevate factors linked to cardiovascular disease, and influence the regulation of inflammatory responses[6]. Cardiac adipose tissue, primarily comprising epicardial adipose tissue

[1]Department of Ultrasound Imaging, the First People's Hospital of Wenling, Wenling City, Zhejiang Province, People's Republic of China. [2]Department of Radiology, Wenling Traditional Chinese Medicine Hospital, Wenling City, Zhejiang Province, People's Republic of China. ✉email: wlyy101292@tzc.edu.cn

(EAT) and paracardial adipose tissue (PAT), is associated with coronary artery calcification, atherosclerotic plaque formation, and coronary artery disease (CAD)[7,8]. EAT, affixed to the myocardium, modulates coronary artery function via inflammatory cytokine secretion and lipid deposition. The thickness of EAT has been shown to correlate significantly with the range and severity of CAD in previous studies[9,10]. This relationship underscores the detection capability of EAT thickness in evaluating coronary artery compromise. On the other hand, PAT, situated between the outer surface of the pericardium and the mediastinal boundary, has also been found to aggravate vascular inflammation and promote the progression of coronary atherosclerosis[11]. Evidence from a study in Korea demonstrated PAT volume is associated with CAD events, even after adjustment for established cardiovascular risk factors[12]. Evidently, EAT and PAT exhibit distinct yet interconnected roles in the pathophysiology of cardiovascular diseases. Consequently, integrating both adipose tissues in stenosis severity assessments is essential for accurate evaluation.

Although coronary computed tomography angiography (CCTA) is a highly regarded tool for the assessment of CAD, it carries inherent disadvantages. These include the necessity for contrast media, which introduces the risk of allergic reactions and nephropathy; heart rate restrictions that may necessitate pre-examination medication to achieve optimal imaging conditions; along with prolonged exposure times and higher costs[13]. By comparison, conventional computed tomography (CT) scans offer the advantage of lower radiation exposure and greater accessibility. Additionally, in assessing cardiac adipose tissue, CT outperforms in terms of temporal and spatial resolution, affording three-dimensional visualization of the heart and epicardial surface and facilitating accurate measurement of adipose tissue volume[14]. Regrettably, previous analyses of cardiac CT images have predominantly relied on basic quantitative metrics, such as fat volume measurements. These parameters, though informative, often fall short of capturing the intricate biomarkers indicative of CAD. The advent of radiomics, utilizing advanced image processing algorithms, represents a significant breakthrough, providing radiologists with analytical tools that are both more accurate and efficient. This method excels in mining extensive, detailed features from imaging data, including shape, texture, and density, across CT and magnetic resonance imaging (MRI) modalities[15,16]. Detailed feature extraction can reveal subtle microstructural changes in adipose tissue, thereby elucidating its functional status without incurring additional costs. This advancement holds the potential to significantly broaden the scope of cardiac CT, moving well beyond the conventional focus on stenosis or calcification, towards a more nuanced understanding of cardiovascular health.

The widespread adoption of machine learning algorithms in recent years has significantly enhanced the analysis and interpretation of detailed data extracted from cardiac CT images, facilitating a deeper understanding of the link between cardiac adiposity and cardiovascular diseases. These algorithms are capable of processing and deciphering complex imaging data, identifying subtle yet diagnostically significant patterns that traditional linear analysis methods often fail to detect[17,18].

Currently, studies on the radiomics of cardiac fat in T2DM patients with NAFLD are still relatively few, and the roles of PAT and EAT in severe coronary artery stenosis have not yet been fully explored. Despite a relative abundance of studies on EAT, integrated analyses of both adipose tissues are uncommon in the existing literature. Additionally, the accuracy and reliability provided by clinical models alone in detecting the presence of cardiovascular diseases are often inadequate, especially in complex cases.

This study aims to address these gaps by evaluating the utility of CT radiomics combined with machine learning in detecting severe coronary artery stenosis. Employing this innovative methodology allows for a comprehensive assessment of the relationship between cardiac fat and coronary stenosis without relying on CCTA. This investigation established radiomics, clinical, and radiomics-clinical models, subsequently comparing their performance in the early detection of high-risk patient groups, thus providing a basis for personalized treatment strategies.

Materials and methods

Subject population

This study conducted a retrospective analysis of data from patients with T2DM and NAFLD, suspected of CAD and evaluated via CCTA, recorded at First People's Hospital of Wenling from January 2020 to December 2023. The diagnostic criteria for T2DM were based on the American Diabetes Association criteria[19]. The diagnosis of NAFLD followed the 2016 Clinical Practice Guidelines for the management of NAFLD[20], incorporating characteristic ultrasonography features while excluding alcohol consumption exceeding 30 g per day for men and 20 g per day for women, as well as other significant liver diseases causing hepatic damage. Additional exclusion criteria included[1]: patients with confirmed CAD or who had undergone percutaneous coronary intervention (PCI) or coronary artery bypass grafting (CABG) before admission[2]; severe hepatic or renal dysfunction, thoracic malignancy, infectious diseases, autoimmune connective tissue diseases[3]; other cardiac conditions (history of myocardial infarction, cardiomyopathy, valvular heart disease, congenital heart disease)[4]; poor image quality or incomplete clinical information. The severity of CAD was assessed using the CAD-RADS classification according to the American College of Cardiology Consensus[21], where CAD-RADS 4 or 5 indicated severe coronary stenosis, and CAD-RADS less than 4 was considered non-severe. A total of 710 patients were included in the study and then were randomly divided into a training set (497 patients) and a validation set (213 patients) by 7:3. The flowchart of the study was shown in Fig. 1.

This study adhered strictly to ethical standards as prescribed by the Declaration of Helsinki, and was approved by the Ethics Review Committee of the First People's Hospital of Wenling (KYY-2024-2008-01). Owing to its retrospective design, the Ethics Review Committee of the First People's Hospital of Wenling provided a waiver for the requirement of informed consent from participants. Measures were taken to anonymize participant data thoroughly prior to analysis, safeguarding their confidentiality and privacy.

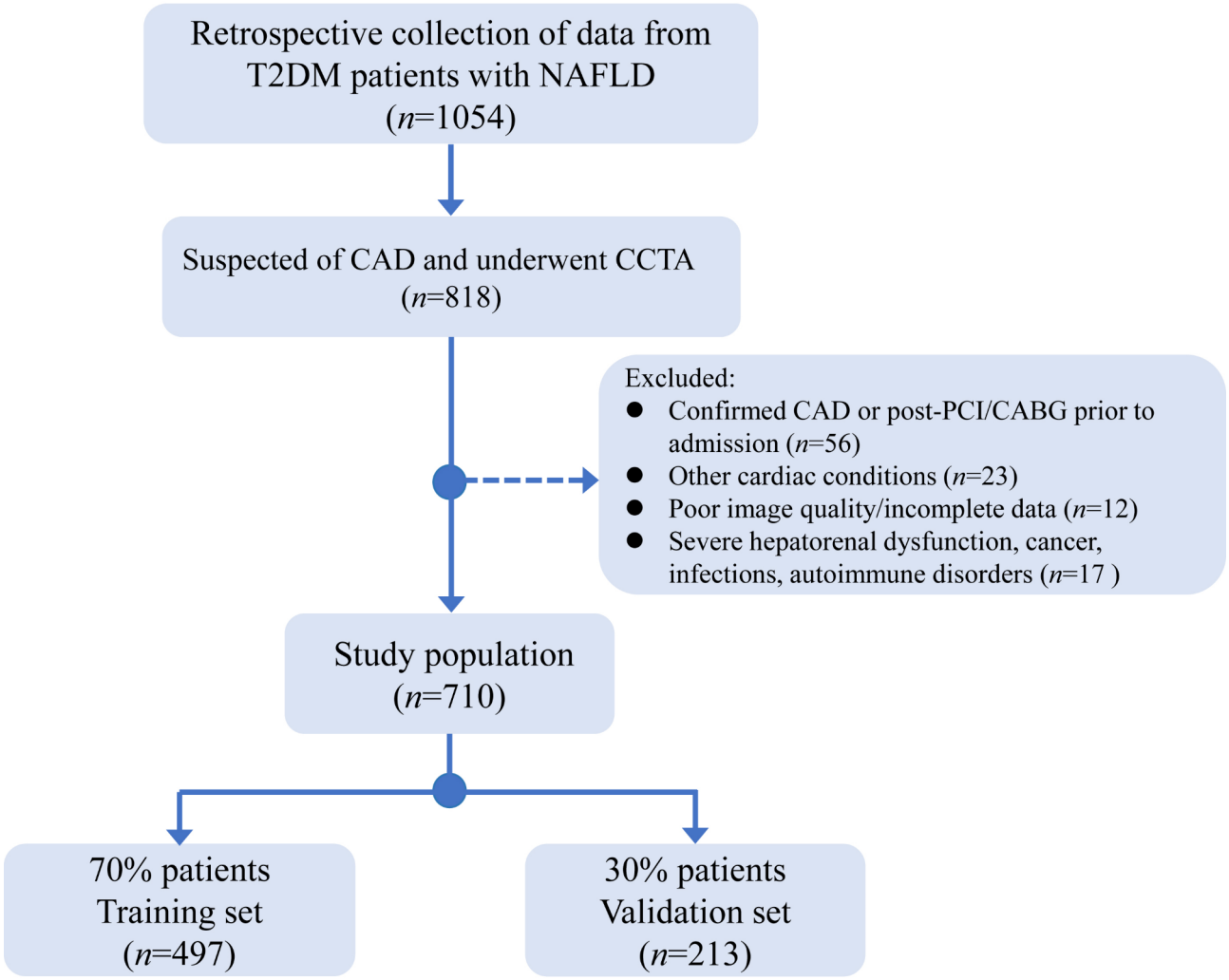

Fig. 1. Flowchart depicting patient selection criteria and process in the study. T2DM, type 2 diabetes mellitus; NAFLD, non-alcoholic fatty liver disease; CAD, coronary artery disease; CCTA, coronary computed tomographic angiography; PCI, percutaneous coronary intervention; CABG, coronary artery bypass grafting.

Information collection

Baseline data were collected from medical records, including gender, age, height, weight, systolic and diastolic blood pressure, smoking history, and family history of CAD. Biochemical test results were also documented, encompassing fasting blood glucose (FBG), glycated hemoglobin (HbA1c), alanine aminotransferase (ALT), aspartate aminotransferase (AST), total cholesterol (TC), triglycerides (TG), high-density lipoprotein cholesterol (HDL-C), and low-density lipoprotein cholesterol (LDL-C).

Smoking status is defined as the consumption of at least five cigarettes daily for over a year. A CAD family history is acknowledged if a direct relative was diagnosed with the disease. Hypertension is specified as a systolic blood pressure ≥ 140mmHg, a diastolic blood pressure ≥ 90mmHg, or the use of antihypertensive drugs before hospital admission. Dyslipidemia criteria include any of the following[22]: TC ≥ 5.2mmol/L, TG ≥ 1.7mmol/L, LDL-C ≥ 3.4mmol/L, HDL-C < 1.0 mmol/L, or being on cholesterol-lowering medications.

Echocardiography

Echocardiographic evaluations were performed on patients with the Doppler ultrasonic diagnostic apparatus (Vivid E95, GE Healthcare, Chicago, USA), with a probe frequency of 1.4 MHz to 4.6 MHz. For each patient, dynamic two-dimensional ultrasound images of three cardiac cycles were captured, specifically in the apical four-chamber, two-chamber, and left ventricular long-axis views. Offline analysis was performed using auto-function imaging 2.0. The ventricular endocardium was automatically outlined by the software and adjusted as needed. Automatic tracking and myocardial segmentation follow, with global longitudinal strain (GLS), global circumferential strain (GCS), and global radial strain (GRS) being documented.

CCTA examination protocol

Quantitative analysis of cardiac fat in T2DM patients with NAFLD was performed using a 64-slice spiral CT (Optima CT680, GE Healthcare, Chicago, USA). Patients were informed about the procedure and precautions, screened for allergies, and required to fast for 6 h prior to scanning to minimize digestive system interference. β-blockers were administered 30 to 40 min before the scan to achieve a heart rate of ≤ 65 beats per minute. Patients were positioned supine with arms raised above the head for the CT scan. Instructions to hold breath during scanning were given to reduce respiratory motion artifacts and improve image quality. The scanning conditions were a tube voltage of 120 kV with automatic tube current adjustment, a slice thickness of 0.625 mm, and a pitch automatically adjusted based on heart rate. Electrocardiogram-gated technology was used to synchronize cardiac movement and imaging, capturing images at times of minimal cardiac motion. Scans spanned from the tracheal bifurcation to the lower edge of the heart, covering the whole heart. Contrast-enhanced scans followed, with 60–80 ml of Iopamiro (370 mg I/mL, Bracco, Milan, Italy) injected at a 4 ml/s flow rate, succeeded by a 40 ml saline flush. An automatic contrast threshold (trigger threshold: 110HU) at the aortic root delayed scanning by 6 s. Fat tissues were differentiated from other tissues within Advantage Workstation 4.6 (GE Healthcare, Chicago, USA) by applying a density range of −190 to −30 Hounsfield Units, the process being independently conducted by experienced radiologists.

Feature extraction

Radiomics analysis of cardiac fat CT images was conducted by two seasoned radiologists using 3D Slicer's Radiomics Extension module for accurate identification and semi-automatic segmentation of EAT and PAT (Fig. 2A-F). Following segmentation, the Radiomics Extension module automatically extracted features from the segmented EAT and PAT regions of interest (ROIs). Radiomic features from each radiologist's segmentation were then averaged into a single value per feature to enhance consistency. Extracted features were categorized into shape features, first-order features, texture features, and advanced texture features, each offering unique insights into the characteristics of cardiac fat.

Shape features quantify the geometry of ROIs, such as volume, surface area, sphericity, and maximum diameters, providing insights into structural changes. First-order features describe voxel intensity distributions within the ROI, including metrics like mean, median, skewness, kurtosis, and entropy, offering a direct assessment of the tissue's signal characteristics. Texture features, also referred to as second-order statistics, evaluate the spatial arrangement of voxel intensities, revealing tissue heterogeneity. Five texture matrices were utilized: gray level co-occurrence matrix (GLCM), describing the joint probability of voxel intensity pairs; gray level run length matrix (GLRLM), assessing the length of consecutive runs of identical intensity values; gray level size zone matrix (GLSZM), quantifying the size distribution of homogeneous intensity zones; gray level dependence matrix (GLDM), evaluating the dependency of voxel intensities on their neighbors; and neighboring gray tone difference matrix (NGTDM), measuring the difference between a voxel's intensity and the average intensity of its surrounding pixels[23].

Advanced texture features capture intricate spatial patterns, elucidating the heterogeneity and subtle structural changes within cardiac adipose tissue. To deepen this analysis, wavelet transform was employed, decomposing images into frequency components through orthogonal filter banks, combining high-pass (H) and low-pass (L) filters across each dimension of three-dimensional cardiac fat CT images[24]. The H filter accentuates intensity variations, enhancing finer details, while the L filter smooths intensity, retaining broader patterns and reducing noise. Each 3D CT volume was thus processed through specific filter combinations, yielding wavelet-domain images with texture details at multiple spatial scales. This multiscale decomposition results in spatially directed frequency channels that characterize localized variations in tissue, with the energy within each channel serving as a distinctive feature. The HHH configuration captures high-frequency details across all directions, while HHL, HLH, and LHH emphasize directional edges and diagonal structures. Configurations such as LLH, LHL, and HLL focus on mid-frequency patterns, highlighting broader structural elements. The LLL combination isolates low-frequency components, representing the overall tissue architecture. This setup provides a comprehensive representation of tissue complexity by preserving fine structural information alongside broader patterns, supporting an in-depth assessment of cardiac adipose tissue[16,25].

Prior to feature extraction, all images were resampled to a voxel size of 1 mm×1 mm×1 mm using nearest-neighbor interpolation. The inter-observer reproducibility of radiomics feature extraction was assessed by calculating the intraclass correlation coefficient (ICC) for 20 cases analyzed independently by both radiologists. Features with an ICC exceeding 0.75 were deemed reliable and selected for further analysis.

Feature selection

During feature selection, features extracted from CT images and relevant clinical indices were standardized using Z-scores. All feature selection processes were conducted exclusively on the training set. Features significantly associated with severe coronary artery stenosis were identified through the Wilcoxon rank-sum test within the training data. Subsequently, the minimum redundancy maximum relevance (mRMR) algorithm was applied to identify features with high relevance to the target variable and low redundancy. Finally, fine feature selection was performed using the least absolute shrinkage and selection operator (LASSO) regression model with 10-fold cross-validation.

Machine learning model

Three detection models were established in this study: clinical model, radiomics model, and combined radiomics-clinical model. The clinical model comprised patient demographics, biochemical indexes, and ultrasound

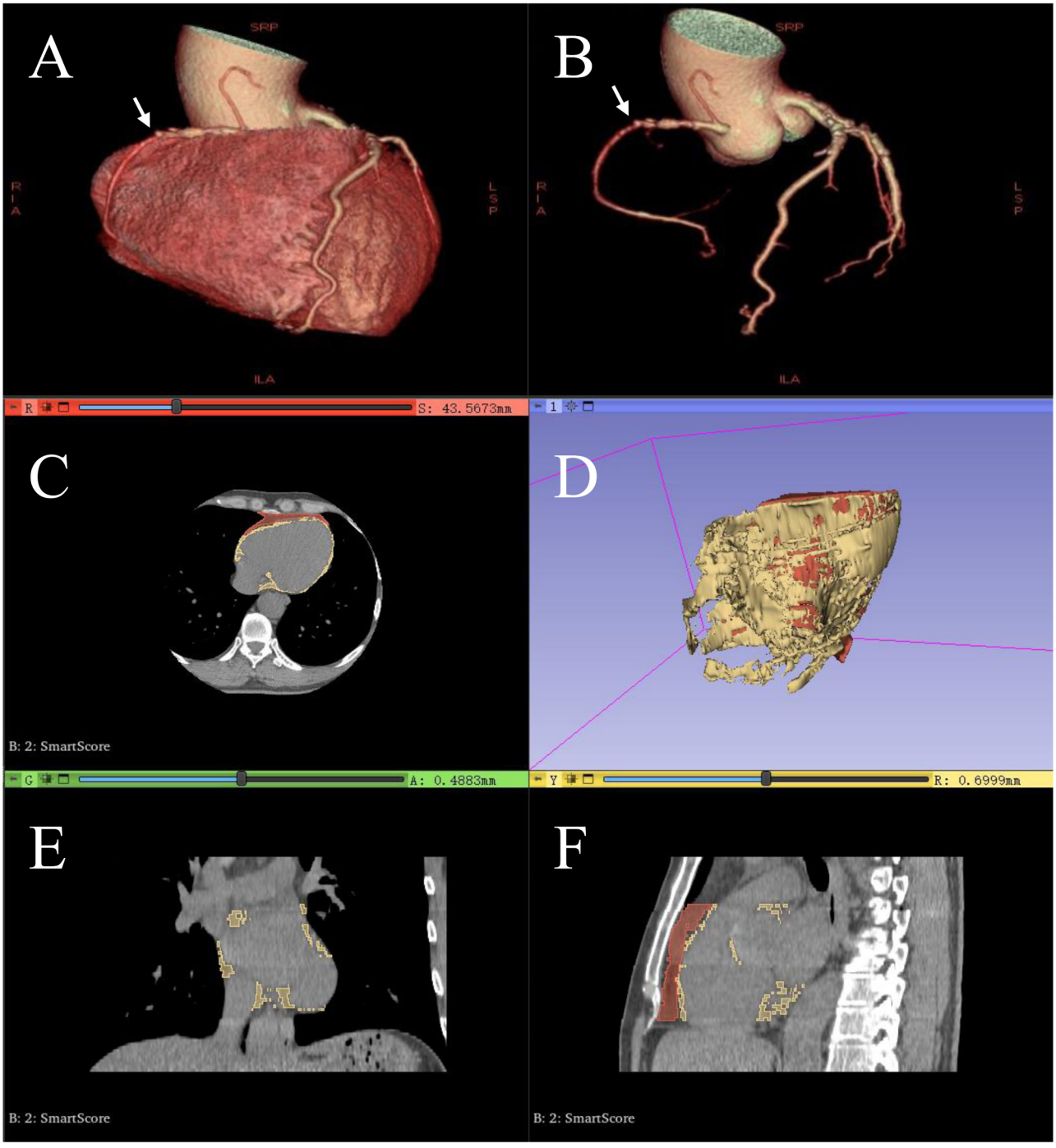

Fig. 2. Coronary imaging and cardiac fat tissue segmentation for a 57-year-old male patient with a CAD-RADS of 4. (A) Tridimensional reconstruction of the heart. White arrow indicates sites of severe stenosis; (B) Volume-rendered coronary tree. White arrow indicates sites of severe stenosis; (C) CT scan axial slice with PAT and EAT, yellow indicates EAT and red indicates PAT; (D) 3D slicer visualization of semi-automated segmentation of cardiac adipose tissue, yellow for EAT and red for PAT; (E) Coronal CT view illustrating segmented cardiac adipose tissue; (F) Sagittal CT reconstruction with mapped cardiac adipose tissue, yellow for EAT and red for PAT. T2DM, type 2 diabetes mellitus; NAFLD, non-alcoholic fatty liver disease; EAT, epicardial adipose tissue; PAT, paracardial adipose tissue; CT, computed tomography.

parameters, whereas the radiomics model utilized features extracted from cardiac fat imaging. The combined model effectively integrated both data sets.

Machine learning algorithms used in model development included random forest (RF), support vector machine (SVM), extreme gradient boosting (XGBoost), and logistic regression. For the RF, variations in the number of trees (100, 300, 500), maximum tree depth[4,6,8], and minimum samples for splitting[2,5,10] were

explored. The SVM explored regularization parameter C at levels (1×10^{-2}, 1×10^{-1}, 1, 10) and evaluated kernels including linear, radial basis function, and polynomial, with tolerance set at 1×10^{-5}, 1×10^{-4}, and $1\times10^{-3}$for model precision enhancement. XGBoost settings adjusted learning rates (0.01, 0.1, 0.2), number of trees (100, 200, 300), and maximum tree depths[3–5] to improve performance. Logistic regression was applied with an L2 regularization approach, assessing the effects of varying regularization strengths (1×10^{-1}, 1, 10). To ensure robust model performance, hyperparameter selection and optimization were conducted on the training set (497 patients) using grid search and 10-fold cross-validation. In this process, the training set was randomly divided into ten subsets, with each subset sequentially serving as a validation fold for hyperparameter tuning, while the remaining nine subsets were used for training. The validation set (213 patients) was reserved exclusively for independent performance assessment and was not used during cross-validation or model tuning. Models were assessed for accuracy, recall, precision, and the area under the receiver operating characteristic (ROC) curve (AUC). The radiomics feature selection and relevant workflow were illustrated in Fig. 3.

Statistical analysis

Statistical analysis was conducted using SPSS (version 26.0, IBM, USA) and Python (version 3.7.6, Python Software Foundation). Continuous variables were compared with Student's t-test or the Mann-Whitney U test, depending on distribution characteristics. Categorical variables were analyzed with chi-square or Fisher's exact test to establish statistical associations. Model calibration was assessed with calibration curves to compare estimated probabilities with actual outcomes. Decision curve analysis (DCA) evaluated the clinical applicability of the models, and the DeLong test compared AUC values across models. Additionally, Shapley Additive exPlanations (SHAP) methodology clarified the contributions of individual variables, enhancing the interpretability of machine learning model outputs. A p-value below 0.05 was deemed statistically significant across all tests.

Results

Basic information

The study included a total of 710 patients, divided into a training set of 497 individuals and a validation set of 213 individuals. Male patients constituted 57.75% ($n=410$) of the study population, with approximately half of the participants having hypertension and 14.08% ($n=100$) having dyslipidemia. All patients underwent CCTA, with severe coronary artery stenosis observed in 95 patients (19.11%) from the training set and 45 patients (21.13%) from the validation set. Baseline characteristics of patients in both the training set and validation set were presented in Table 1, showing no statistically significant differences between the groups ($P>0.05$).

CT radiomics features extraction

From the CT images of each participant, 1316 EAT features and 1316 PAT features were extracted, including first-order statistics ($n=108$), shape features ($n=14$), texture features ($n=450$), and wavelet features ($n=744$), respectively. Initially, features with an ICC below 0.75 were removed, totaling 292 features. The Wilcoxon rank-sum test was then applied, retaining 123 radiomics features for EAT and 130 for PAT. The mRMR algorithm further reduced the features for EAT and PAT to 20 each. Ultimately, dimensionality reduction using LASSO regression identified 5 radiomics features for EAT and 5 for PAT with non-zero coefficients, illustrated in Fig. 4A-D.

Performance of different models in the training set

In the radiomics analysis of cardiac fat tissue CT imaging, the XGBoost algorithm demonstrated the highest detection performance, achieving an AUC of 0.838, followed by RF, with SVM and logistic regression showing lower AUC values (Fig. 5A). Calibration and DCA analyses further confirmed XGBoost's superior accuracy and

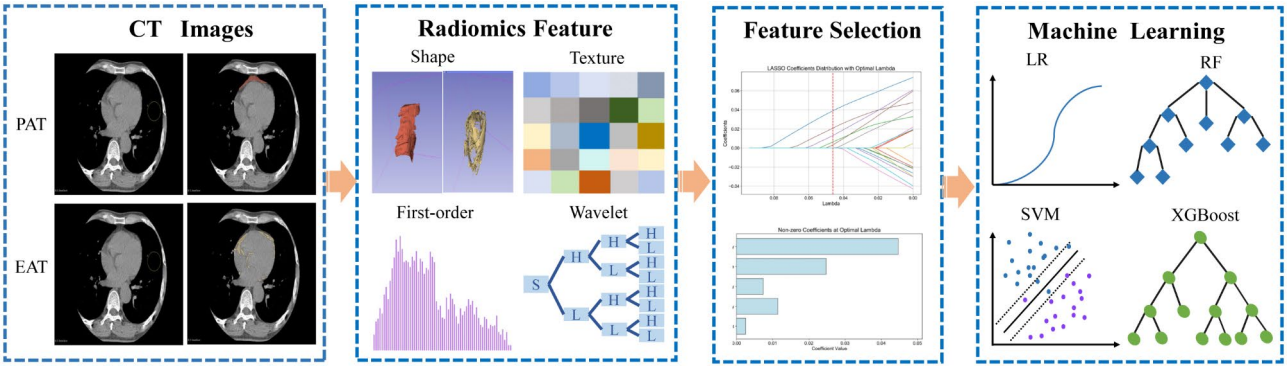

Fig. 3. Radiomics and machine learning workflow for coronary stenosis detection in T2DM with NAFLD, including image acquisition and segmentation, radiomics feature extraction, feature selection, and model development with machine learning. CT, computed tomography; T2DM, type 2 diabetes mellitus; NAFLD, non-alcoholic fatty liver disease; EAT, epicardial adipose tissue; PAT, paracardial adipose tissue; LR, logistic regression; RF, random forest; SVM, support vector machine; XGBoost, extreme gradient boosting.

Characteristic	Training set ($n=497$)	Validation set ($n=213$)	P value
Age, years	56.98 ± 10.23	58.05 ± 13.04	0.242
Gender, %male	289 (58.15%)	121 (56.81%)	0.740
Diabetes duration, years	7.66 ± 2.90	7.71 ± 2.97	0.835
BMI, kg/m^2	26.52 ± 4.08	26.33 ± 4.40	0.579
Current smokers, %	144 (28.97%)	66 (30.99%)	0.59
Hypertension, %	254 (51.11%)	104 (48.83%)	0.578
Dyslipidemia, %	75 (15.09%)	25 (11.74)	0.239
Family history, %	42 (8.5%)	21 (9.9%)	0.545
Severe stenosis, %	95 (19.11%)	45 (21.13%)	0.537
Biochemcal indexes			
FBG, mmol/L	8.42 ± 2.20	8.44 ± 2.17	0.911
HbA1c, %	7.49 ± 0.89	7.52 ± 0.88	0.68
TC, mmol/L	4.36 ± 0.74	4.34 ± 0.72	0.739
LDL-C, mmol/L	2.80 ± 0.85	2.82 ± 0.82	0.772
HDL-C, mmol/L	1.29 ± 0.42	1.26 ± 0.40	0.377
TG, mmol/L	1.95 ± 0.50	1.93 ± 0.55	0.636
ALT, U/L	37.58 ± 10.99	38.61 ± 10.41	0.245
AST, U/L	28.59 ± 9.37	29.32 ± 9.16	0.339
Ultrasound parameter			
E/A	1.11 ± 0.31	1.10 ± 0.29	0.688
Lateral e', cm/s	13.31 ± 2.22	13.46 ± 2.28	0.413
Septal e', cm/s	11.51 ± 1.75	11.45 ± 1.64	0.67
Average E/e'	10.28 ± 2.48	10.53 ± 2.61	0.226
LVDd, mm	44.90 ± 3.90	45.28 ± 3.32	0.215
LVDs, mm	29.57 ± 3.14	29.36 ± 2.99	0.408
LVEF, %	59.99 ± 3.57	59.79 ± 3.85	0.504
GLS, %	16.21 ± 3.09	16.35 ± 2.84	0.571
GRS, %	35.27 ± 3.34	35.18 ± 3.10	0.737
GCS, %	20.43 ± 2.45	20.51 ± 2.76	0.701

Table 1. Baseline characteristics and clinical data of patients in the training set and validation set. BMI, body mass index; FBG, fasting blood glucose; HbA1c, glycated hemoglobin; TC, total cholesterol; LDL-C, and low-density lipoprotein cholesterol; HDL-C, high-density lipoprotein cholesterol; TG, triglycerides; ALT, alanine aminotransferase; AST, aspartate aminotransferase; E, early diastolic transmitral flow velocity; A, atrial systolic transmitral flow velocity; e', early diastolic tissue velocity; LVDd, left ventricular diastolic diameter; LVDs, left ventricular systolic diameter; LVEF, left ventricular ejection fraction; GLS, global longitudinal strain; GRS, global radial strain; GCS, global circumferential strain.

net benefit for clinical decision-making (Fig. 5B and C). For clinical variables, logistic regression achieved the highest AUC but showed a lower net benefit in DCA curves. SVM demonstrated an AUC of 0.747 with favorable calibration and DCA results, making it suitable for the clinical model (Fig. 5D and E, and 5F).

The combined radiomics-clinical model enhanced detection capability, with the XGBoost algorithm achieving optimal results, including a high AUC, better calibration, and the highest net benefit in DCA curves, outperforming the RF algorithm (Fig. 5G and H, and 5I). Compared to the single clinical and radiomics models, the radiomics-clinical model excelled on the training set, with an AUC of 0.883 and an accuracy of 0.906 (Table 2).

Performance of different models in the validation set

In the validation set, the radiomics model utilizing the XGBoost algorithm exhibited solid detection performance, with an AUC of 0.787. The calibration curve for this model displayed moderate agreement with the ideal line, while DCA curves revealed limited net benefit across certain thresholds, suggesting restricted applicability (Fig. 6A-C). For clinical model, based on the SVM algorithm, yielded an AUC of 0.719. Analysis of its calibration curve showed noticeable deviations from the ideal line at higher predicted probabilities, and DCA curves demonstrated minimal net benefit across the threshold range (Fig. 6D-F). The radiomics-clinical model maintained consistent detection performance across training and validation sets, achieving an AUC of 0.852 and an accuracy of 0.845 in the validation set. This model's calibration curve was well-aligned with the ideal line, and DCA curves indicated a substantial net benefit across a broad range of thresholds, underscoring its clinical utility (Fig. 6G-I). Compared to the individual clinical and radiomics models, the combined model provided the highest metrics overall, with an F1 score of 0.507, recall of 0.378, and precision of 0.773 (Table 2).

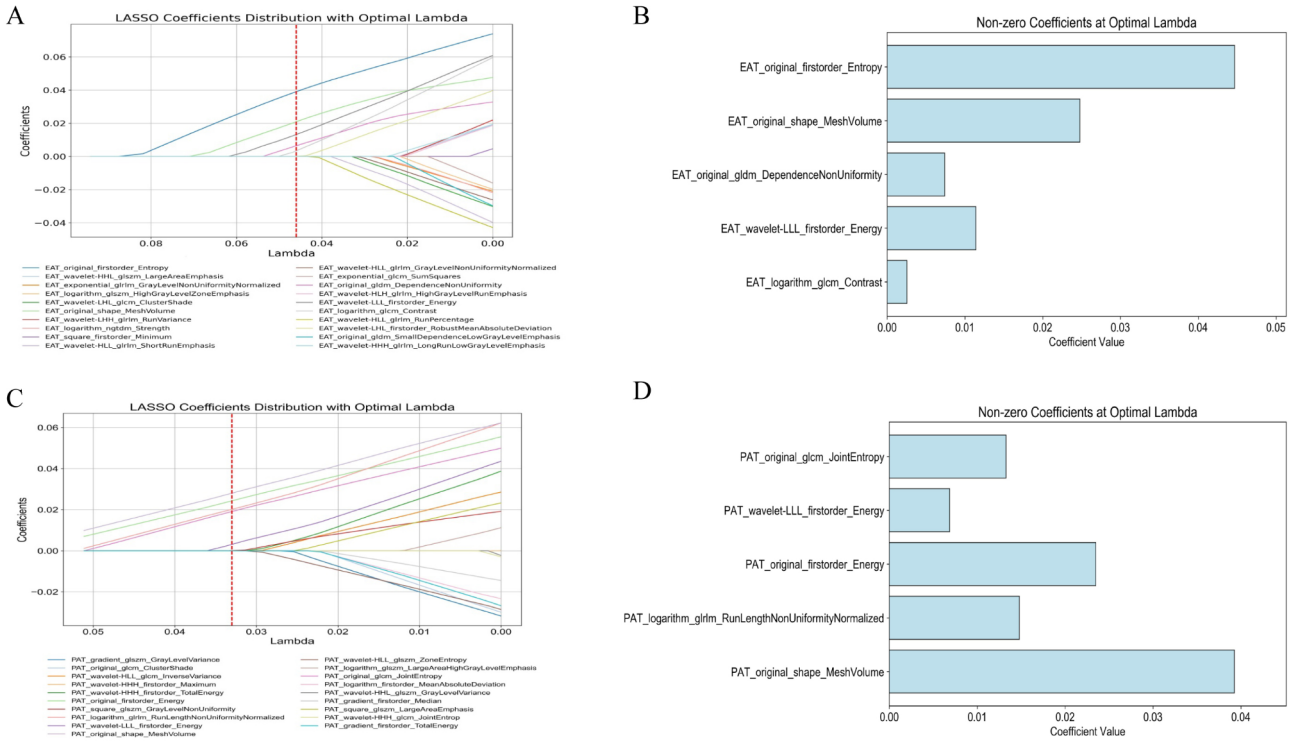

Fig. 4. Radiomics feature selection of cardiac adipose tissue identified by LASSO regression with tenfold cross-validation. (A) LASSO coefficient profiles of EAT radiomics features. The red vertical line shows the best λ value that resulted in 5 features with non-zero coefficients; (B) Contribution of five EAT features with non-zero coefficients to radiomics and their respective coefficients. (C) LASSO coefficient profiles of PAT radiomics features. The red vertical line shows the best λ value that resulted in 5 features with non-zero coefficients; (D) Contribution of five PAT features with non-zero coefficients to radiomics and their respective coefficients. LASSO, least absolute shrinkage and selection operator; EAT, epicardial adipose tissue; PAT, paracardial adipose tissue.

Interpretability features of radiomics-clinical model

SHAP plots were utilized to elucidate the degree of contribution of each feature to the model performance. As depicted in Fig. 7A, features such as EAT_original_shape_MeshVolume, EAT_original_firstorder_Entropy, and PAT_original_shape_MeshVolume emerged as notably influential to the model output. Additionally, clinical data including diabetes duration, GLS, and LDL-C also played crucial roles in model detection. In Fig. 7B, the distribution of SHAP values for each feature illustrated the individualized contribution differences to the model's detection, with points transitioning from blue to pink indicating a change from low to high feature values.

Discussion

Accurate detection of severe coronary artery stenosis (> 70%) is imperative for effective cardiovascular risk stratification in patients with T2DM concomitant with NAFLD. Severe stenosis exerts a substantial impact on cardiac perfusion when contrasted with moderate stenosis (50%), potentially precipitating myocardial ischemia or myocardial infarction. Research data have shown that over 90% of acute myocardial infarction cases present with coronary artery stenosis exceeding 50%, and among these, a majority exceed 70% stenosis[26]. At thresholds beyond 70% stenosis, the myocardial blood supply may become critically insufficient, increasing the likelihood of acute cardiovascular incidents. Consequently, the early detection and management of severe stenosis are essential in preventing acute cardiac events among this demographic.

In this study, a combination of cardiac CT radiomics analysis and clinical data was employed to develop multiple machine learning models, including RF, SVM, logistic regression, and XGBoost. The present study revealed that the combined radiomics-clinical model (utilizing the XGBoost algorithm) excelled in detecting severe coronary artery stenosis, outperforming both single models in terms of AUC, accuracy, and other critical performance metrics. Furthermore, SHAP analysis highlighted the significant impact of features such as the original shape volume of EAT, original first-order entropy of EAT, original shape volume of PAT, diabetes duration, and GLS on the detection models. These findings underscore the value of merging radiomics features with clinical data, introducing an advanced tool for assessment in clinical cardiology, with the potential to minimize the dependency on contrast media. Implementing this model could enhance strategies for cardiac health management, particularly benefiting patient groups inadequately served by conventional assessment techniques.

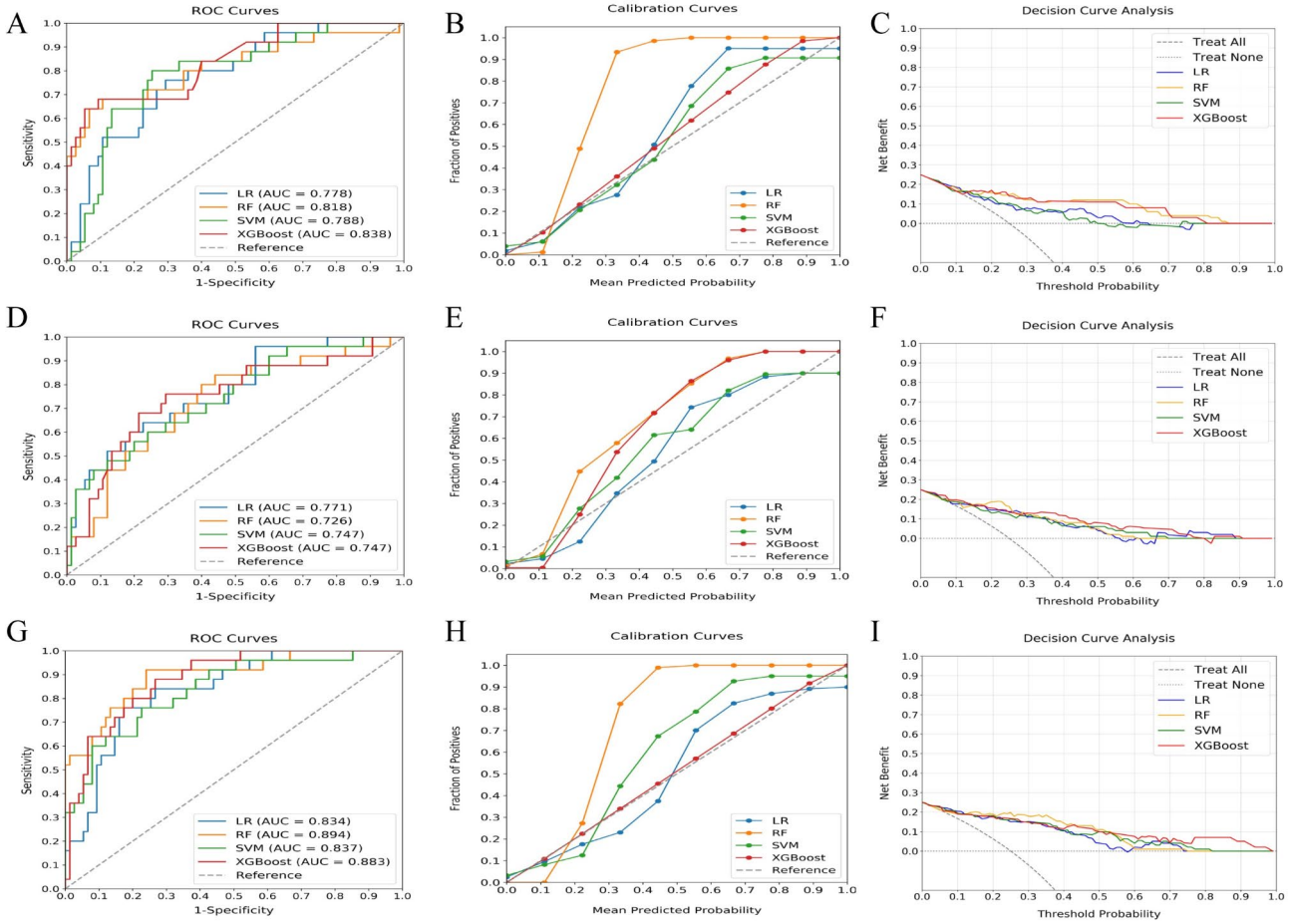

Fig. 5. Detection performance of radiomic, clinical, and combined feature models in the training set. (A) ROC curves of the radiomics model in the training set; (B) Calibration curves of the radiomics model in the training set; (C) DCA curves of the radiomics model in the training set; (D) ROC curves of the clinical model in the training set; (E) Calibration curves of the clinical model in the training set; (F) DCA curves of the clinical model in the training set. (G) ROC curve of the radiomics-clinical model in the training set; (H) Calibration curves of the radiomics-clinical model in the training set; (I) DCA curves of the the radiomics-clinical model in the training set. LR, logistic regression; RF, random forest; SVM, support vector machine; XGBoost, extreme gradient boosting; ROC, receiver operating characteristic curves; AUC, Area under the curve; DCA, decision curve analysis.

Metrics	Datasets	Radiomics model	Clinical model	Radiomics-clinical model
AUC	Training set	0.838 (0.715–0.902)	0.747 (0.667–0.827)*	0.883 (0.779–0.943)*#
	Validation set	0.787 (723-0.851)	0.719 (0.655–0.783)*	0.852 (0.792–0.912)*#
Accuracy	Training set	0.815	0.723	0.906
	Validation set	0.831	0.798	0.845
F1	Training set	0.702	0.648	0.771
	Validation set	0.500	0.157	0.507
Recall	Training set	0.681	0.716	0.765
	Validation set	0.400	0.089	0.378
Precision	Training set	0.733	0.592	0.780
	Validation set	0.677	0.667	0.773

Table 2. Performance comparison of different models in detection of severe coronary stenosis. AUC, area under the curve. *$p < 0.05$ compare with radiomics model; #$p < 0.05$ compare with clinical model.

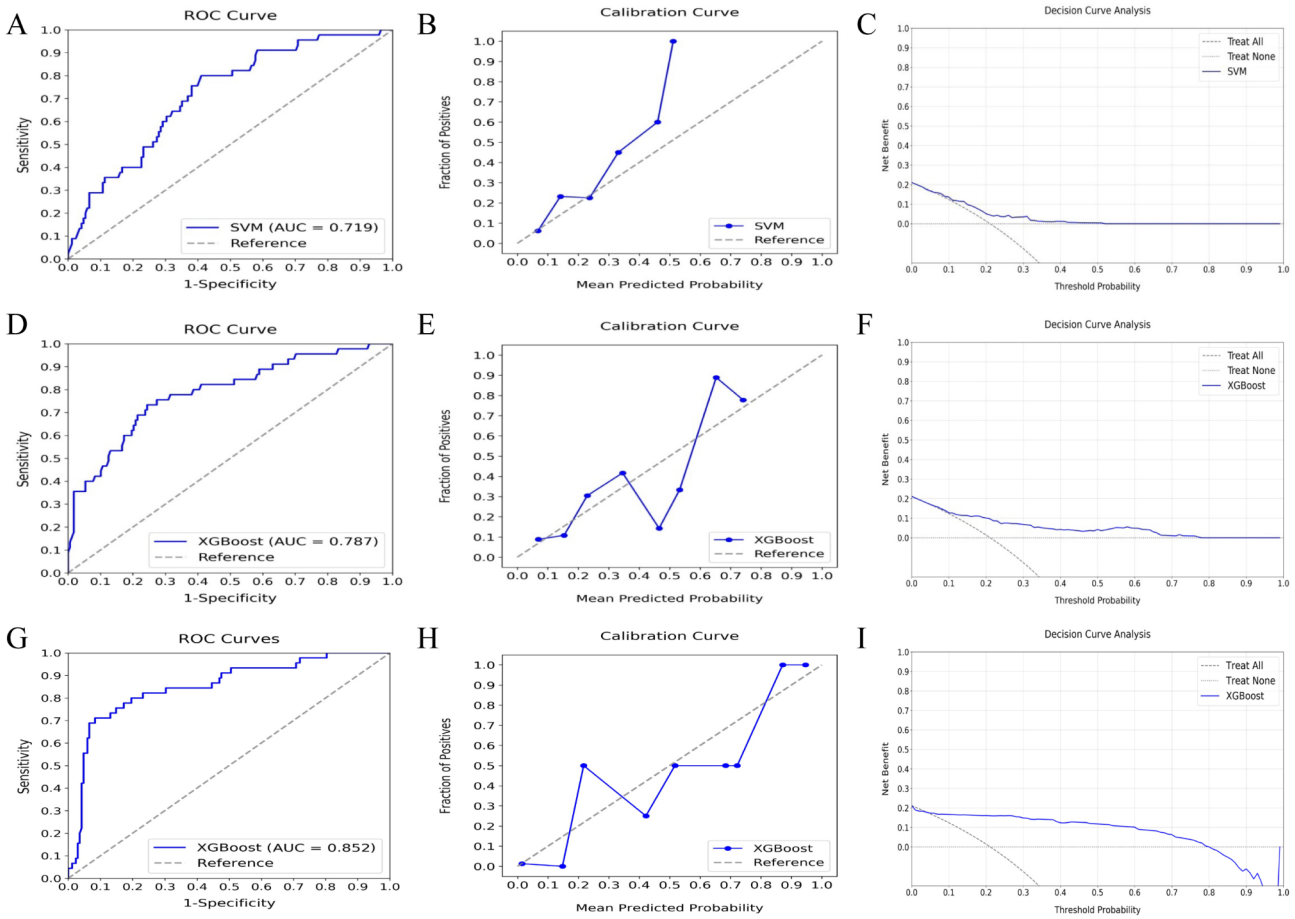

Fig. 6. Performance of radiomics, clinical, and combined radiomics-clinical models in the validation set for disease assessment. (A) ROC curve of the XGBoost-based radiomics model in the validation set; (B) Calibration curves of XGBoost-based radiomics model in the validation set; (C) DCA curves of XGBoost-based radiomics model in the validation set; (D) ROC curve of the SVM-based clinical model in the validation set; (E) Calibration curve of the SVM-based clinical model in the validation set; (F) DCA curves of the SVM-based clinical model in the validation set. (G) ROC curve of the radiomics-clinical model with XGBoost in the validation set; (H) Calibration curve of the radiomics-clinical model with XGBoost in the validation set; (I) DCA curves of the radiomics-clinical model with XGBoost in the validation set. LR, logistic regression; RF, random forest; SVM, support vector machine; XGBoost, extreme gradient boosting; ROC, receiver operating characteristic curves; AUC, Area under the curve; DCA, Decision curve analysis.

NAFLD and T2DM coexist due to shared metabolic risk factors and exhibit a synergistic effect, leading to adverse cardiovascular events. Risk factors such as disease duration, age, hypertension, LDL-C, and HbA1c are implicated in the development of moderate to severe coronary artery stenosis[27,28]. Although conventional risk factors are widely used for quantifying the probability of cardiovascular events, prevailing assessment models, including the 2013 American College of Cardiology (ACC)/ American Heart Association (AHA) risk equation, may overestimate the risk, resulting in unnecessary medication prescriptions and highlighting the need for improved model accuracy[29]. In this study, a model for detecting severe coronary artery stenosis was developed using clinical variables. The SVM within the clinical model achieved an AUC of 0.747 on the ROC, indicating some discriminative ability. However, the model's performance, particularly at higher detection probabilities, was suboptimal, as demonstrated by calibration and DCA curves, revealing notable deviations from the ideal. This underscores the limitations of relying solely on individual clinical variables for detection, suggesting the necessity of a comprehensive analysis involving multidimensional data.

The accumulation of visceral fat, especially the aberrant distribution of cardiac fat, emerges as a critical factor exacerbating the risk of CAD in individuals with T2DM and NAFLD[30,31]. EAT, a metabolically active organ, has garnered attention in cardiovascular disease research due to its close anatomical relation to the heart and coronary arteries. Previous cross-sectional investigations have elucidated a correlation between EAT volume and intra-abdominal visceral fat, establishing EAT volume as a contributor to the development of CAD[32,33]. PAT, enveloping the heart's outer surface, constitutes approximately 20–50% of the heart's mass. Recent research showed that PAT volume is the optimal indicator for assessing the severity of coronary artery disease, compared to waist circumference or visceral abdominal fat volume[34]. Other studies also further confirmed that an elevated

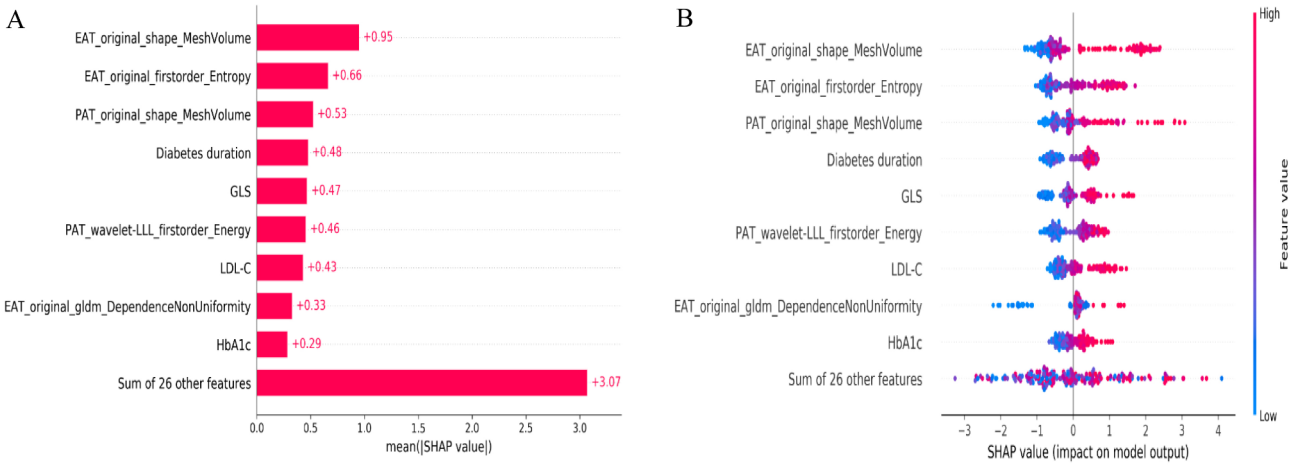

Fig. 7. Radiomics-clinical model interpretation using SHAP. (A) Mean SHAP values of top features in radiomics-clinical models. Bars indicate the mean absolute SHAP values, quantifying the average contribution of the top features to the model's detection performance. (B) SHAP value beeswarm plot of top features in radiomics-clinical models. Each point represents the SHAP value of a patient feature. Pink has a positive effect on the detection and blue has a negative impact. The horizontal axis measures the SHAP value's effect on model output, and the vertical axis displays the features ranked by their mean absolute SHAP values.

volume of PAT is associated with atherosclerosis, low adiponectin levels, and inflammation, identifying it as a risk factor for CAD[35]. Indeed, due to distinct anatomical locations and potential differences in biological mechanisms, EAT and PAT are commonly subjected to separate analyses in multiple studies. However, they collectively constitute the primary adipose tissue within the heart, potentially exerting a concerted influence on the health status of the coronary arteries. Therefore, a combined analysis of both EAT and PAT holds the promise of providing a more comprehensive assessment of cardiovascular disease. Christensen et al.[36] conducted an analysis involving 200 T2DM patients with elevated urinary albumin excretion rates but without known CAD. They found that individuals with lower cardiac fat exhibited a reduced risk of cardiovascular disease and mortality compared to those with higher levels of cardiac fat. Cardiovascular disease events and overall mortality were correlated with total cardiac fat rather than individually measured EAT or PAT. It is worth emphasizing that most studies typically focus solely on fat volume, neglecting to thoroughly explore the nuanced information within the images.

The advancement of radiomics has introduced novel research avenues in this domain. As an advanced imaging analysis technique, radiomics provides a nuanced perspective on the intricate interplay between cardiac adipose tissue and CAD by extracting a series of intricate features[37]. In this study, radiomics analysis of EAT and PAT respectively revealed five key features, including first-order statistics, shape-based features, and advanced texture features. These features may be indicative of pathological alterations in cardiac adipose tissue. First-order statistics primarily delineate the distribution and variability of pixel intensities within adipose tissue. Shape features offer insights into the relative size of the image array, with larger values signifying increased adipose volume, reflecting the cumulative extent of adipose tissue. Numerous studies have confirmed a positive association between the volumes of EAT and PAT and the severity of CAD, establishing them as reliable markers for cardiovascular condition assessment[38]. Recently, Szabo et al.[39] proposed that radiomics features derived from the texture and shape of PAT can discern and predict heart failure. From a pathophysiological perspective, the excessive accumulation of both types of cardiac adipose tissue results in deleterious lipotoxicity and the generation of inflammatory factors. The secretion of these inflammatory factors promotes the formation of atherosclerosis, triggering vascular dysfunction, diminishing the bioactivity of oxidative phosphorylation enzymes, ultimately resulting in both organic and functional damage to the cardiovascular system. This study analyzed these features using machine learning models and found that the XGBoost demonstrated good performance in detecting severe coronary artery stenosis, achieving an AUC of 0.787 in the validation set. This outcome suggests that the integration of radiomics features with machine learning algorithms can effectively identify indicators associated with CAD. Notably, compared to the model based only on clinical variables, radiomics model provides more comprehensive information, contributing to enhanced accuracy in CAD detection. This finding aligns with similar observations in the study conducted by Yu et al.[40], further confirming the crucial role of cardiac adipose tissue features in assessing cardiovascular diseases.

Subsequently, we integrated clinical features into the radiomics model, developing a radiomics-clinical model to enhance detection performance. Results from this study indicate that the comprehensive model achieves greater accurately in identifying severe coronary artery stenosis, outperforming both the clinical and radiomics models across the training and, notably, validation sets. In the training set, the XGBoost algorithm demonstrated superior performance in the calibration curve and DCA curve compared to the RF algorithm, likely attributed to its efficiency in handling complex datasets and accurately capturing interactions between different features[41]. This aligns with recent assessments of machine learning algorithms in medical diagnostics. The high AUC value and accuracy of the radiomics-clinical model validate its effectiveness in clinical decision support, especially

in precision medicine. In the validation set, the radiomics-clinical model demonstrated an AUC of 0.852 and an accuracy of 0.845, underscoring the clinical utility of integrating radiomics with clinical data. Improved calibration and net benefit in DCA curves across a range of thresholds emphasize the model's potential utility for CAD detection in clinical settings. Together, these findings confirm the XGBoost algorithm's robust generalization in the validation set, further affirming the model's stability and clinical applicability. Importantly, the interpretable model proposed in this study elucidates how the identified features impact endpoint events, significantly enhancing physicians' understanding of the connection between the identified features and the model. The ultimately selected clinical features, such as diabetes duration, GLS, LDL-C, and HbA1c, align with the conclusions of Lu et al.[42] and others, underscoring the reliability of the identified features. For high-risk patients with T2DM and NAFLD, local interpretations of single-patient assessments can be achieved using SHAP plots. This model facilitates monitoring and early identification of CAD in the subclinical period, reducing the cardiovascular burden and mortality risk for T2DM patients with NAFLD.

This study has several limitations and prospects. Firstly, its retrospective and single-center design may introduce inherent selection biases, potentially impacting the broader applicability of the findings. Future research should therefore prioritize adopting a multi-center, prospective approach to bolster the external validity of these conclusions. Secondly, all images were obtained from a single CT scanner, which improves consistency in imaging conditions within this dataset but may limit generalizability due to potential variability in radiomics features across different scanners. Incorporating data from multiple centers with varied imaging protocols and equipment will be critical to validate the robustness and reproducibility of radiomics features across different settings. Although the sample size of 710 individuals is relatively large compared to similar studies, further increasing the sample size across diverse centers would strengthen the robustness of the findings. Furthermore, the segmentation process for cardiac fat in CT images involves a degree of subjectivity, posing implications for the precision and consistency of radiomics data. The advent of automated segmentation through advanced techniques like deep learning holds promise for enhancing the objectivity and efficiency of data processing. Finally, despite the promising detection capabilities exhibited by initial machine learning models, their development relies on a singular dataset without independent external validation, presenting challenges to their generalizability. Future studies should focus on external validation and explore the model's utility across diverse populations and clinical contexts to improve both its practicality and accuracy.

In conclusion, the integration of cardiac fat radiomics with clinical data, utilizing the XGBoost algorithm, suggests a promising method for detecting severe coronary artery stenosis. SHAP analysis highlights key factors, offering fresh insights into cardiac health evaluation. This approach could improve patient care by reducing the need for contrast agents and refining clinical decision-making processes.

Data availability statement

All data generated during this study are included in this article. Further enquiries can be directed to the corresponding author.

Received: 27 March 2024; Accepted: 20 February 2025
Published online: 25 February 2025

References

1. Tanase, D. M. et al. The Intricate Relationship between Type 2 Diabetes Mellitus (T2DM), Insulin Resistance (IR), and Nonalcoholic Fatty Liver Disease (NAFLD). *Journal of Diabetes Research*. 2020:3920196. (2020). https://doi.org/10.1155/2020/3920196
2. Muzica, C. M. & Sfarti, C. Nonalcoholic Fatty Liver Disease and Type 2 Diabetes Mellitus: A Bidirectional Relationship. 2020:6638306. (2020). https://doi.org/10.1155/2020/6638306
3. Cho, E. E. L. et al. Global prevalence of non-alcoholic fatty liver disease in type 2 diabetes mellitus: an updated systematic review and meta-analysis. *Gut* **72** (11), 2138–2148. https://doi.org/10.1136/gutjnl-2023-330110 (2023).
4. Alshumrani, G. A. Coronary artery calcium score above 250 confirms the presence of significant stenosis in coronary CT angiography of symptomatic patients. *Coron. Artery Dis.* **33** (3), 189–195. https://doi.org/10.1097/mca.0000000000001082 (2022).
5. Zhang, H-W. et al. Association of diabetes mellitus with clinical outcomes in patients with different coronary artery stenosis. *Cardiovasc. Diabetol.* **20** (1), 214. https://doi.org/10.1186/s12933-021-01403-6 (2021).
6. Sato, F. et al. Association of epicardial, visceral, and subcutaneous fat with cardiometabolic diseases. *Circ. J.* **82** (2), 502–508. https://doi.org/10.1253/circj.CJ-17-0820 (2018).
7. Lang, Y., Wei, F. & Fan, Y. Cardiac adipose tissue is associated with coronary artery disease: a meta-analysis. *Int. J. Cardiol.* **176** (2), 567–570. https://doi.org/10.1016/j.ijcard.2014.07.006 (2014).
8. Liu, J. et al. Association of epicardial and pericardial adipose tissue volumes with coronary artery calcification. *Int. Heart J.* **63** (6), 1019–1025. https://doi.org/10.1536/ihj.22-006 (2022).
9. Ahn, S. G. et al. Relationship of epicardial adipose tissue by echocardiography to coronary artery disease. *Heart* **94** (3), e7. https://doi.org/10.1136/hrt.2007.118471 (2008).
10. Eroglu, S. et al. Epicardial adipose tissue thickness by echocardiography is a marker for the presence and severity of coronary artery disease. *Nutr. Metab. Cardiovasc. Dis.* **19** (3), 211–217. https://doi.org/10.1016/j.numecd.2008.05.002 (2009).
11. Kim, T. H. et al. Pericardial fat amount is an independent risk factor of coronary artery stenosis assessed by multidetector-row computed tomography: the Korean atherosclerosis study 2. *Obes. (Silver Spring)*. **19** (5), 1028–1034. https://doi.org/10.1038/oby.2010.246 (2011).
12. Ueda, Y. et al. Association between the presence or severity of coronary artery disease and pericardial fat, paracardial fat, epicardial fat, visceral fat, and subcutaneous fat as assessed by Multi-Detector row computed tomography. *Int. Heart J.* **59** (4), 695–704. https://doi.org/10.1536/ihj.17-234 (2018).
13. Nance, J. W. Jr., Bamberg, F. & Schoepf, U. J. Coronary computed tomography angiography in patients with chronic chest pain: systematic review of evidence base and cost-effectiveness. *J. Thorac. Imaging.* **27** (5), 277–288. https://doi.org/10.1097/RTI.0b013e3182631c5c (2012).
14. Mazonakis, M. & Damilakis, J. Computed tomography: what and how does it measure? *Eur. J. Radiol.* **85** (8), 1499–1504. https://doi.org/10.1016/j.ejrad.2016.03.002 (2016).

15. Lambin, P. et al. Radiomics: the Bridge between medical imaging and personalized medicine. *Nat. Rev. Clin. Oncol.* **14** (12), 749–762. https://doi.org/10.1038/nrclinonc.2017.141 (2017).
16. Ayx, I., Froelich, M. F., Baumann, S., Papavassiliu, T. & Schoenberg, S. O. Radiomics in Cardiac Computed Tomography. *Diagnostics*. 13(2):307. (2023).
17. Al'Aref, S. J. et al. Clinical applications of machine learning in cardiovascular disease and its relevance to cardiac imaging. *Eur. Heart J.* **40** (24), 1975–1986. https://doi.org/10.1093/eurheartj/ehy404 (2019).
18. Mathur, P., Srivastava, S., Xu, X. & Mehta, J. L. Artificial intelligence, machine learning, and cardiovascular disease. *Clin. Med. Insights Cardiol.* **14**, 1179546820927404. https://doi.org/10.1177/1179546820927404 (2020).
19. Association, A. D. 2. Classification and diagnosis of diabetes: standards of medical care in Diabetes—2019. *Diabetes Care*. **42** (Supplement_1), S13–S28. https://doi.org/10.2337/dc19-S002 (2018).
20. European Association for the Study of the L. European association for the study of D, European association for the study of O. EASL–EASD–EASO clinical practice guidelines for the management of non-alcoholic fatty liver disease. *Diabetologia* **59** (6), 1121–1140. https://doi.org/10.1007/s00125-016-3902-y (2016).
21. Cury, R. C. et al. An expert consensus document of the Society of Cardiovascular Computed Tomography (SCCT), the American College of Radiology (ACR) and the North American Society for Cardiovascular Imaging (NASCI). Endorsed by the American College of Cardiology. *J. Cardiovasc. Comput. Tomogr.* **10** (4), 269–281. https://doi.org/10.1016/j.jcct.2016.04.005 (2016). CAD-R ADS(TM) Coronary Artery Disease - Reporting and Data System.
22. revision Jcfg. Chinese guidelines for the management of dyslipidemia in adults. *J Geriatr Cardiol*. (2018) 15(1):1–29. (2016). https://doi.org/10.11909/j.issn.1671-5411.2018.01.011
23. Ge, G. & Zhang, J. Feature selection methods and predictive models in CT lung cancer radiomics. *J. Appl. Clin. Med. Phys.* **24** (1), e13869. https://doi.org/10.1002/acm2.13869 (2023).
24. Liu, Z. et al. Radiomics signature of epicardial adipose tissue for predicting postoperative atrial fibrillation after pulmonary endarterectomy. *Front. Cardiovasc. Med.* **9**, 1046931. https://doi.org/10.3389/fcvm.2022.1046931 (2022).
25. Mayerhoefer, M. E. et al. Introduction to radiomics. *J. Nucl. Med.* **61** (4), 488–495. https://doi.org/10.2967/jnumed.118.222893 (2020).
26. Ambrose, J. A. et al. Angiographic progression of coronary artery disease and the development of myocardial infarction. *J. Am. Coll. Cardiol.* **12** (1), 56–62. https://doi.org/10.1016/0735-1097(88)90356-7 (1988).
27. Younossi, Z. M. et al. The global epidemiology of NAFLD and NASH in patients with type 2 diabetes: A systematic review and meta-analysis. *J. Hepatol.* **71** (4), 793–801. https://doi.org/10.1016/j.jhep.2019.06.021 (2019).
28. Fujii, H., Kawada, N. & Japan Study Group Of Nafld J-N. The role of insulin resistance and diabetes in nonalcoholic fatty liver disease. *Int. J. Mol. Sci.* **21** (11). https://doi.org/10.3390/ijms21113863 (2020).
29. Muntner, P., Safford, M. M., Cushman, M. & Howard, G. Comment on the reports of over-estimation of ASCVD risk using the 2013 AHA/ACC risk equation. *Circulation* **129** (2), 266–267. https://doi.org/10.1161/circulationaha.113.007648 (2014).
30. Yun, C. H. et al. Pericardial and thoracic peri-aortic adipose tissues contribute to systemic inflammation and calcified coronary atherosclerosis independent of body fat composition, anthropometric measures and traditional cardiovascular risks. *Eur. J. Radiol.* **81** (4), 749–756. https://doi.org/10.1016/j.ejrad.2011.01.035 (2012).
31. Wu, F. Z., Wu, C. C., Kuo, P. L. & Wu, M. T. Differential impacts of cardiac and abdominal ectopic fat deposits on cardiometabolic risk stratification. *BMC Cardiovasc. Disord.* **16**, 20. https://doi.org/10.1186/s12872-016-0195-5 (2016).
32. Monti, C. B. et al. Novel imaging biomarkers: epicardial adipose tissue evaluation. *Br. J. Radiol.* **93** (1113), 20190770. https://doi.org/10.1259/bjr.20190770 (2020).
33. Cosson, E. et al. Epicardial adipose tissue volume and coronary calcification among people living with diabetes: a cross-sectional study. *Cardiovasc. Diabetol.* **20** (1), 35. https://doi.org/10.1186/s12933-021-01225-6 (2021).
34. Jeong, J. W. et al. Echocardiographic epicardial fat thickness and coronary artery disease. *Circ. J.* **71** (4), 536–539. https://doi.org/10.1253/circj.71.536 (2007).
35. Greif, M. et al. Pericardial adipose tissue determined by dual source CT is a risk factor for coronary atherosclerosis. *Arterioscler. Thromb. Vasc Biol.* **29** (5), 781–786. https://doi.org/10.1161/atvbaha.108.180653 (2009).
36. Christensen, R. H. et al. Epicardial, pericardial and total cardiac fat and cardiovascular disease in type 2 diabetic patients with elevated urinary albumin excretion rate. *Eur. J. Prev. Cardiol.* **24** (14), 1517–1524. https://doi.org/10.1177/2047487317717820 (2017).
37. Ueno, K. et al. Increased epicardial fat volume quantified by 64-multidetector computed tomography is associated with coronary atherosclerosis and totally occlusive lesions. *Circ. J.* **73** (10), 1927–1933. https://doi.org/10.1253/circj.cj-09-0266 (2009).
38. Homayounieh, F. et al. Prediction of coronary calcification and stenosis: role of radiomics from Low-Dose CT. *Acad. Radiol.* **28** (7), 972–979. https://doi.org/10.1016/j.acra.2020.09.021 (2021).
39. Szabo, L. et al. Radiomics of pericardial fat: a new frontier in heart failure discrimination and prediction. *Eur. Radiol.* https://doi.org/10.1007/s00330-023-10311-0 (2023).
40. Yu, W. et al. Machine learning to predict hemodynamically significant CAD based on traditional risk factors, coronary artery calcium and epicardial fat volume. *J. Nuclear Cardiol.* **30** (6), 2593–2606. https://doi.org/10.1007/s12350-023-03333-0 (2023).
41. Dinh, A., Miertschin, S., Young, A. & Mohanty, S. D. A data-driven approach to predicting diabetes and cardiovascular disease with machine learning. *BMC Med. Inf. Decis. Mak.* **19** (1), 211. https://doi.org/10.1186/s12911-019-0918-5 (2019).
42. Lu, H., Zeng, L., Liang, B., Shu, X. & Xie, D. High prevalence of coronary heart disease in type 2 diabetic patients with non-alcoholic fatty liver disease. *Arch. Med. Res.* **40** (7), 571–575. https://doi.org/10.1016/j.arcmed.2009.07.009 (2009).

Acknowledgements

Not applicable.

Funding

This work was supported by Wenling Social Development Science and Technology Projects (2022S00145, 2024S00219).

Declarations

Conflict of interest statement

The authors have no conflicts of interest to declare.

Ethical approval

This study was approved by the Ethics Review Committee of the First People's Hospital of Wenling (KYY-2024-2008-01).

Informed consent
Informed consent was waived by the Ethics Committee of the First People's Hospital of Wenling due to the study's retrospective design.

Contributors
The study was conceived and designed by M.L. and W.H. Data collection was performed by M.L., L.F., and W.H., with statistical analysis conducted by M.L., and X.C. M.L. and W.H. was responsible for drafting the manuscript. All authors reviewed the manuscript.

Additional information
Correspondence and requests for materials should be addressed to W.H.

Reprints and permissions information is available at www.nature.com/reprints.

Publisher's note Springer Nature remains neutral with regard to jurisdictional claims in published maps and institutional affiliations.